https://doi.org/10.5194/tc-2023-8
Preprint. Discussion started: 7 February 2023
© Author(s) 2023. CC BY 4.0 License.

The Cryosphere Discussions

Brief Communication: Effects of different saturation vapor pressure calculations on simulated surface-subsurface hydrothermal regimes at a permafrost field site

Xiang Huang, Charles J. Abolt, and Katrina E. Bennett
Earth and Environmental Sciences, Los Alamos National Laboratory, Los Alamos, NM, 87545 USA

Correspondences: Xiang Huang (xhuang@lanl.gov)

Abstract Air saturation vapor pressure (SVP) can be calculated using different formulas, with or without over-ice correction. These different approaches result in variability that affects the simulation of surface-subsurface thermal-hydrological processes in cold regions; however, this topic has not been well documented to date. In this study, we compared the relative humidity (RH) downloaded and calculated from four data sources in Alaska based on five commonly used SVP formulas. RH, along with other meteorological indicators, was used to drive physically-based land surface models. Results show that RH is a sensitive parameter, and its variations from SVP with or without over-ice correction meaningfully impact model-based predictions of snow depth, sublimation, soil temperature, and active layer thickness.

Keywords: Relative humidity, air saturation vapor pressure, observations, cold regions, Alaska, Arctic

1 Introduction

Near-surface air humidity is a term used to describe the amount of water vapor (moisture) in the lowermost portion of the atmosphere. Water vapor is an essential meteorological variable for characterizing environmental and climatic system changes (Gill, 1982; Dessler & Sherwood, 2009). Because water vapor can condense into liquid water or be deposited as solid ice, humidity is a measurement of the latent heat stored/released in the air, which can strongly affect atmospheric stability and influences dynamical processes in the atmosphere-vegetation-soil system. Depending on the measurement method used, water vapor can be expressed in several forms, such as relative humidity (RH, the amount of water vapor in the air relative to the maximum amount possible), specific humidity (SH, the mass of water vapor per unit mass of air), absolute humidity (AH, the mass of water vapor in a volume of air), mixing ratio (the mass of water vapor compared to the mass of dry air), or dew point temperature (the temperature at which the air becomes saturated when the specific humidity remains constant). These variables can be used interchangeably with additional knowledge of air pressure and air temperature, the latter of which can be used to estimate saturation vapor pressure (SVP) or the maximum vapor pressure that the air can support (Gill, 1982).

Humidity variables that appear in publications or databases have frequently been converted using different empirical formulations of the SVP (e.g., Westermann et al., 2016; Brauner et al., 2019). However, the SVP formulation used is often not reported, which may result in errors of interpretation, as different formulations incorporate different assumptions. Although

https://doi.org/10.5194/tc-2023-8
Preprint. Discussion started: 7 February 2023
© Author(s) 2023. CC BY 4.0 License.


many attempts have been made to compare the relative errors among different SVP formulations (e.g., Alduchov & Eskridge, 1996; Xu et al., 2012; Vömel, 2016), the degree to which the magnitude and dissemination of these errors affect meteorological analysis is largely unknown. Therefore, it is necessary to evaluate the impacts of different SVP formulations on humidity variables to reveal the links and feedbacks between water vapor and thermal dynamics, which are a crucial part of simulating cold-region climate phenomena accurately, particularly when considering climate change projection using earth system models.

In most cases, variations of humidity (e.g., corrections, biases) receive less attention compared with air temperature, air pressure, and precipitation (snowfall and rainfall) when publishing meteorological datasets and/or collecting forcings or input data to land surface models (e.g., Li et al., 2017; Xie et al., 2022). These variations can come from observational errors and calculation (conversion) errors, such as the choices of expressions for the SVP over a surface of water or ice when humidity is reported as RH. While the variations introduced by conversion errors are usually more minor than the observational errors, they both introduce systematic inaccuracies in humidity data. The value of the SVP over ice is smaller than that over water because the molecular forces bind much more tightly in an ice crystal than in the liquid water phase (Gill, 1982; Alduchov & Eskridge, 1996). However, the SVP is often calculated only over the water surface in many cold region studies (e.g., Xu et al., 2012; Valiantzas, 2013; Leppäranta, 2015; Li et al., 2017; Brauner, 2019; Nian et al., 2022; Xie et al., 2022), and the influences of differences in SVP over water and ice on the calculation of the humidity variable are not generally evaluated in these studies. Moreover, the impact of calculating RH due to incorrect calculation of the SVP (with or without respect to the ice surface) on hydrological analysis has not been comprehensively investigated. How these choices affect the surface-subsurface thermal-hydrological processes in cold regions is a poorly studied topic of considerable interest.

In this study, we compared RH data downloaded directly from the ERA5-land, CRN (NOAA), and Barrow Environmental Observatory (BEO) datasets near Utqiagvik, Alaska, with the RH derived from the specific humidity variable reported in GLDAS (NASA), employing five commonly used formulas for calculating the SVP. Then, the RH data were used to drive a permafrost column land surface model using the Advanced Terrestrial Simulator (ATS) (Coon et al., 2019) to examine the responses exhibited within a typical Arctic tundra site. The simulated soil temperature profiles, snow depth, sublimation, and active layer thickness were comparably analyzed and discussed. Overall, our findings improved the quality assurance/quality checking (QA/QC) for the humidity datasets and provided valuable insights for landscape-scale projections of permafrost dynamics under a warming climate.

2 Data and methods

2.1 Forcing datasets

Four meteorological forcing datasets near Utqiagvik, Alaska, were tested in this study. The daily relative humidity (RH), air temperature, rain precipitation, snow precipitation, incoming shortwave radiation, incoming longwave radiation, and wind

https://doi.org/10.5194/tc-2023-8
Preprint. Discussion started: 7 February 2023
© Author(s) 2023. CC BY 4.0 License.


speed meteorological forcing data were accessed from the (1) reanalysis dataset ERA5-land (accessed: https://www.ecmwf.int/en/era5-land), (2) observational dataset CRN (NOAA) (accessed: https://www.ncei.noaa.gov/access/crn/qcdatasets.html), and (3) observational dataset at the Barrow Environmental Observatory (BEO) (Atchley et al., 2015; Jan et al., 2020). The daily specific humidity (SH), along with six other meteorological variables, were downloaded from the (4) reanalysis dataset GLDAS (NASA) (accessed: https://disc.gsfc.nasa.gov/information/tools?title=Hydrology%20Data%20Rods). A comparison in Figure S1 (see Supplement Material) shows these different data have a generally good agreement between them except for a few discrepancies in rates of rainfall and snowfall. For comparison with the other datasets and for use in our model, SH from GLDAS was converted to RH based on the following equations:

$$RH = \frac{e_a\left(P_a - e_s\right)}{e_s\left(P_a - e_a\right)} \times 100\% \approx \frac{e_a}{e_s} \times 100\% \tag{1}$$

$$SH = \frac{e_a \kappa}{P_a + e_a(1-\kappa)} \tag{2}$$

where e_s is the SVP and e_a is the water vapor pressure (Pa) in the air; P_a is the surface (local) air pressure (Pa); and κ is the ratio of the molar weights of water vapor and dry air (κ=0.622). In addition to the above-mentioned humidity variables (RH and SH), absolute humidity (AH) has also appeared in the literature (e.g., Leppäranta, 2015; Westermann et al., 2016) and is expressed as a function of temperature (°C) and % RH based on the ideal gas law using the following equation (Harpold & Brooks, 2018):

$$\mathrm{AH} = \left(\mathrm{RH} \times 6.112 \times e^{\frac{17.67 \times T}{T+243.5}} \times 2.1674\right) \Big/ \left(273.15 + T\right) \tag{3}$$

where the unit of AH is g/m^3 and T is the temperature in °C.

2.2 The SVP formulas

The water SVP is a function of air temperature, which provides a basis for determining other thermodynamic properties of moist air (humidity ratio, specific entropy, specific volume, etc.). There has been much research on formulating the SVP, and dozens of formulas have appeared in the literature (e.g., Alduchov & Eskridge, 1996; Xu et al., 2012; Vömel, 2016), which vary in accuracy and computational efficiency, depending on the temperature ranges and the approximation method of the Clausius-Clapeyron equation. A comprehensive review of all SVP formulas is beyond the scope of this study, and here only the five commonly used formulas are examined.

https://doi.org/10.5194/tc-2023-8
Preprint. Discussion started: 7 February 2023
© Author(s) 2023. CC BY 4.0 License.


2.2.1 Goff-Gratch formula

The internationally accepted formula for calculating the SVP is that of Goff & Gratch (1946) for air temperatures between -50 °C and 102 °C. For a planar surface of pure water and ice, the Goff-Gratch formula is expressed as (e.g., Murray, 1967):

$$\log_{10} e_s = \begin{cases} a_1\left(\frac{373.16}{T}-1\right)+b_1\log_{10}\left(\frac{373.16}{T}\right)+c_1\left[10^{d_1(1-T/373.16)}-1\right]+e_1\left[10^{f_1(373.16/T-1)}\right]+\log_{10} g_1, & T>0^oC \\ a_2\left(\frac{273.16}{T}-1\right)+b_2\log_{10}\left(\frac{273.16}{T}\right)+c_2\left(1-\frac{T}{273.16}\right)+\log_{10} d_2, & T<0^oC \end{cases} \quad (4)$$

where e_s is the SVP in hPa and temperature T in K. The empirical coefficients $a_1 \sim g_1$ and $a_2 \sim d_2$ are defined as: a_1=-7.90298, b_1=5.02808, c_1=1.3816×10^{-7}, d_1 = 11.344, e_1=8.1328×10^{-3}, f_1=-3.49149, g_1=1013.246; a_2=-9.09718, b_2=-3.56654, c_2=0.876793, d_2=6.1071. While the Goff-Gratch formula is demonstrated to have high accuracy (e.g., Alduchov & Eskridge, 1996; Vömel, 2016), it is tedious and inconvenient for use in many applications of calculating the SVP. Therefore, simpler empirical formulas have been developed, and these formulations are applied in many research studies.

2.2.2 August-Roche-Magnus formula

A widely used method for calculating the SVP by the hydrometeorological community is that of Magnus; this formula was modified and later re-named as August-Roche-Magnus formula (e.g., Alduchov & Eskridge 1996; Westermann et al., 2016), which is expressed as:

$$e_s = \begin{cases} 6.11\times e^{17.62T/(T+243.12)}, & T>0^oC \\ 6.11\times e^{22.46T/(T+272.62)}, & T<0^oC \end{cases} \quad (5)$$

where e_s is the SVP in hPa and temperature T in °C. The coefficient 6.11 denotes the reference SVP at a certain temperature, usually 0 °C, and the other coefficients are determined via empirical polynomial fits. Unlike the Goff-Gratch formula, the August-Roche-Magnus formula is simple in structure and highly accurate; as such, this formula is more commonly applied in permafrost research studies (e.g., Westermann et al., 2016).

2.2.3 Buck formula

Buck used a minimax fitting procedure to derive a relatively simple equation for calculating the SVP of water (from 0 °C to 50 °C) and of ice (from -50 °C to 0 °C) as below (Buck, 1981):

https://doi.org/10.5194/tc-2023-8
Preprint. Discussion started: 7 February 2023
© Author(s) 2023. CC BY 4.0 License.


$$e_s = \begin{cases} 6.112 \times e^{T(18.678 - T/234.5)/(T+257.14)}, & T > 0^oC \\ 6.112 \times e^{T(23.306 - T/333.7)/(T+279.82)}, & T < 0^oC \end{cases} \quad (6)$$

where e_s is the SVP in hPa and temperature T in °C. According to Mackay et al. (2017), the Buck formula is the most appropriate SVP formulation for use in cold region studies.

2.2.4 Tetens's formula

The structure of Tetens's formula is similar to the Magnus form. Interestingly, this short equation (over the water surface or without over-ice correction) is considered a general form to calculate the SVP for all temperature ranges and is also commonly used in the literature (e.g., Xu et al., 2012; Valiantzas, 2013; Nian et al., 2022), as below:

$$e_s = 6.11 \times e^{17.27T/(T+237.3)} \quad (7a)$$

where e_s is the SVP in hPa and temperature T in °C. However, some studies have argued that the above Eq. (7a) should only be applied to calculate the SVP over water surfaces (T>0 °C), and a different equation (with over-ice correction) should be used for over-ice surfaces (T<0 °C) (e.g., Murray, 1967; Liu et al., 2021). The over-ice form is expressed as below:

$$e_s = 6.11 \times e^{21.87T/(T+265.5)}, \quad T < 0^0C \quad (7b)$$

According to Murray (1967), the combination of Eqs. (7a) and (7b) for Tetens's formula are within 0.1 % of the Goff-Gratch calculations for temperatures -10 °C and above, and within 1 % for temperatures between -30 °C and -10 °C. This formula is acceptable for most meteorological purposes.

2.2.5 Wexler formula

To get a simple and robust equation for calculating the SVP, one-half of the Wexler formula (over the water surface or without over-ice correction) is also used for all temperature ranges in several studies (e.g., Li et al., 2017; Brauner, 2019; Xie et al., 2022), as below:

$$\log_{10} e_s = \frac{0.7859 + 0.03477T}{1.0 + 0.00412T} \quad (8a)$$

where e_s is the SVP in hPa and temperature T in °C. However, some studies suggest a correction term should be added to the calculation of the SVP over a surface of ice (e.g., Gill, 1982; Leppäranta, 2015); i.e., if the air temperature is below zero, the corrected SVP is expressed as below:

https://doi.org/10.5194/tc-2023-8
Preprint. Discussion started: 7 February 2023
© Author(s) 2023. CC BY 4.0 License.


$$\log_{10} e_s = \frac{0.7859 + 0.03477T}{1.0 + 0.00412T} + 0.00422T, \quad T < 0^0C \tag{8b}$$

2.3 Model description and settings

We used the Advanced Terrestrial Simulator (ATS v1.2) to explore how permafrost dynamics are affected by variability in RH associated with the choice of formulas for estimating SVP described in the previous section (Coon et al., 2019). ATS's permafrost configuration simultaneously solves for the surface and subsurface balance of energy and water mass; it is driven by meteorological forcing data (forcing variables include air temperature, longwave radiation, shortwave radiation, wind speed, rainfall, snowfall, and relative humidity) and allows for the accumulation of snow, ice, and liquid water at the surface, and has been extensively validated against field measurements in previous studies (e.g., Atchley et al., 2015; Abolt et al., 2020; Jan et al., 2020). We constructed a 1D permafrost column model (39 m depth) with a groundwater table close to the ground surface tailored for a tundra field site near Utqiagvik, Alaska. The top twenty centimeters of the column were occupied by organic-rich soils, while the rest of the column comprised mineral soil.

To produce an initial permafrost column, bottom-up freezing of the one-dimensional (1D) variably-saturated unfrozen soil column model was run to a steady-state under a bottom boundary temperature of −9.0 °C and a no flux on the top boundary. After applying these boundary conditions for 1000 simulated years, ATS generated a frozen column with 0.2 m depth of partially-frozen variably-saturated in the upper domain and 38.8 m depth of fully-frozen ice-saturated in the lower domain. The frozen column was then used as an initial condition for multiple simulations, which were (top-down) forced by site-specific annual cyclic meteorological data for the years 2010-2016. Other ATS settings, including the mesh and solver configuration, follow the descriptions in Atchley et al. (2015) and Jan et al. (2020). The workflows are graphically shown in Figure S2 (see Supplement Material), and the key parameters are listed in Table S1. An ensemble of simulations was driven using 13 alternative meteorological forcing datasets. In addition to three datasets in which relative humidity was provided at the time of download (ERA5-land, CRN, and BEO), we used 10 GLDAS-based datasets, in which we converted the SH to RH by taking into account the five SVP formulas with and without over-ice correction.

3 Results and Discussion

3.1 Comparison of RH among forcing datasets

Based on the above formulas for calculating the SVP for the GLDAS dataset, two cases were considered. In Case #1, all five formulas are used over the liquid water surface, which means that the equations for T>0 °C were applied for the whole temperature range. In Case #2, all five formulas are used over both water and ice, i.e., the equations for T>0 °C and for T<0 °C were calculated separately. According to the conversion Eqs. (1) and (2), we estimated RH values from the documented

https://doi.org/10.5194/tc-2023-8
Preprint. Discussion started: 7 February 2023
© Author(s) 2023. CC BY 4.0 License.


SHs of the GLDAS dataset, then compared the results with RH from other data sources (i.e., ERA-5 Land, BEO, and CRN) near Utqiavik.

Figure 1 compares the time series of RH at our field site from 2010-2016 generated for both cases. During the summer period, the GLDAS-derived estimates of RH are identical among the two cases because the conversion equations used are identical for the status of T>0 °C. Still, they show meaningful discrepancies against the RH values from the other data sources, such as the BEO, CRN (NOAA), and ERA5-land. For Case #2 in Figure 1b, with over-ice correction, there are markedly larger values of the RH during the winter period (T<0 °C) than those without over-ice correction in Case #1 (Figure 1a). Differences between Case #2 conversions can be up to 20%. These greater RHs during the winter are caused by the smaller SVP over the ice surface because fewer molecules of ice sublimate to vapor than molecules of water evaporate (e.g., Gill, 1982).

Most of the RH values during the water in Case #2 are larger than 100 %, which indicates super-saturation with water vapor. A similar issue of spurious model humidity values is discussed by Ruosteenoja et al. (2017) in the context of RH with respect to ice, and they found RH values considerably higher than 100 % are common in high latitudes in cold climates. For Case #2 in Figure 1b, during the winter period (T<0 ºC), the calculated RH values are very close to each other for the Goff-Grach, August-Roche-Magnus, and Wexler formulas, while the Tetens formula estimate is slightly higher (+4%). The largest estimated RH (+10%) is from the Buck formula. It can also be seen in Figure 1a that all RH values generally present a positive relationship with the air temperature, while in Figure 1b, the converted RHs from GLDAS dataset show a negative pattern against the air temperature. This negative relationship between the near-surface air RH and air temperature is consistent with the findings in many previous studies (e.g., Leppäranta, 2015; Sexstone et al., 2018). The reason for the inverse relation between RH and air temperature is that the SVP increases with temperature concurrent with reduced RHs and vice versa—for example, during the winter, the smaller SVPs results in the larger RHs.

3.2 Snowpack and sublimation modelling uncertainty

The converted RH, along with the other six forcing variables, were used to drive the land surface model in ATS. Figure 2 presents the simulated snowpack corresponding to the Buck, Tetens, and Wexler formulas with and without over-ice correction alongside observations from the BEO (see the dots in Figure 2). The BEO observations are collected at the center and trough of one typical ice-wedge polygon at the field site. Results using the Goff-Crach and August-Roche-Magnus formulas are omitted, as they are visually indistinguishable from the Wexler formula. It can be seen from Figure 2 that the simulated snow depths are significantly impacted by different forcing datasets. For example, the ERA5-land dataset shows a remarkable under-prediction of the snow depth, while the BEO dataset has the largest predicted values of snow depth. The BEO dataset generally indicates a good agreement with observations from October 2013 to May 2014. However, an exact agreement between simulated and observed snow depths is challenging, as the simulation was conducted on a soil column with a flat surface, while the observed snowpack was impacted by local microtopography (e.g., Atchley et al., 2015; Jan et al., 2020; Abolt et al., 2020).

https://doi.org/10.5194/tc-2023-8
Preprint. Discussion started: 7 February 2023
© Author(s) 2023. CC BY 4.0 License.


Therefore, we can conclude that the snow dynamics can be impacted by minor discrepancies between the forcing variables (see Figure S1 in Supplement Material).

It can also be found from Figure 2 that the greater values of snow depths were predicted for calculating the SVP with over-ice correction than those without over-ice correction for the GLDAS dataset. These greater snow depths are caused by the higher RHs and possible lower sublimations by calculating SVP with the over-ice correction during winter. Compared with the other formulas for the SVP over water and ice, the Buck formula (corresponding to the largest RH values in Case #2) shows the largest values of the snow depth prediction. Both the Tetens formula and the Wexler formula share very close magnitudes and variability (changing patterns) over the winter season of the predicted snow depth.

3.3 Surface-subsurface hydrothermal regimes

To explore in greater depth the degree to which variability in RH used to drive simulations impacts the surface energy balance and thermal dynamics in the surface-subsurface, Figures 3a and 3b present a comparison of the simulated snow depth, sublimation, and thaw depth focusing on the GLDAS forcing dataset with RH values converted using the Wexler formula and Buck formula for the SVP with or without over-ice correction, respectively. The choice to calculate RH with or without an over-ice correction resulted in differences in snow depth of up to 0.13 and 0.18 m based on the Wexler and Buck formulas, respectively. Over the time period from 2010-2016, this corresponded to a difference of 30-40 cm in cumulative sublimation. For the SVP calculating over the ice (with over-ice correction), the temperatures at a depth of 0.1 to 0.5 m were warmer during the winter by up to 2 ^{o}C (see Figure S3 in Supplement Material) because of the thermal resistance of the thick snowpack (Figure 3a and 3b). These findings demonstrate that the variability of the RH exerts substantial impacts on predicted snow depth and hence, winter ground temperatures, which are consistent with the augments in previous studies (Harpold & Brooks, 2018; Sexstone et al., 2018).

It should be noted that these profound impacts on surface and subsurface hydrologic and thermal regimes caused by the errors (variabilities) in humidity from the SVP calculations with or without over-ice correction are not limited to the winter, but can persist throughout the summer under some special conditions. Figure 3c and 3d show the propagation of the predicted thawing front (0 ^{o}C isotherms or the active layer thickness) for the years 2010-2016, when the rain rate increased by five times, causing a shallow surface water body (< 1.0 m deep) to accumulate at the surface. In these figures, i) the thickness of the active layer is strongly impacted by the SVP calculations with or without over-ice correction when substantial ponded water exists, and ii) the Buck formula has larger residuals (up to 0.18 m) of the active layer thickness than those (up to 0.12 m) using the Wexler formula for the SVP calculations with or without over-ice correction. This effect is similar to findings reported by Abolt et al. (2020), who found that thaw depths beneath small ponds become increasingly sensitive to snow depth from the winter prior when the water passes a depth threshold. It occurs because freezing processes in winter slow down markedly when snow accumulates on top of a water body whose surface has frozen. Beneath ponds greater than a few decimetres deep, ground

https://doi.org/10.5194/tc-2023-8
Preprint. Discussion started: 7 February 2023
© Author(s) 2023. CC BY 4.0 License.


temperatures at the end of winter remain several degrees warmer than they would be otherwise, allowing for deeper thaw during the subsequent summer.

4 Concluding remarks

Based on the analyses of the errors (variabilities) in humidity due to the different SVP calculations that were used to drive a physically-based permafrost column land surface model, the following conclusions can be made:

(1) Near-surface humidity is a sensitive parameter for predicting snow depth, and its evolving pattern and magnitude should be carefully considered before applying it within a land surface model if it is downloaded from different sources.

(2) Greater values of the RH are obtained if the SVP was calculated with over-ice correction compared to without during the winter. Compared with the other four commonly used formulas for calculating the SVP, the Buck formula generates the largest RHs over the ice in winter for the conversion of the SHs from the GLDAS dataset.

(3) If the SVP is calculated without over-ice correction, there are significant under-estimation of snow depths (~0.1 m), over-estimation of snow sublimation (~0.3 m), and colder soil temperature (~2 ºC) during the winter freezing period. During the summer thawing period, the choice of whether or not to employ an over-ice correction corresponds to significant variability in simulated thaw depths (~0.18 m) if ponded water is present at the surface.

To avoid physical inconsistencies in humidity variables, the SVP should be corrected over the ice surface when a conversion between the RH, SH, and AH is required in cold climates. Ongoing studies include the uncertainty/sensitivity analyses of the effects of errors in humidity on the dynamics of carbon and other nutrients within a 2D/3D model domain.

Code and data availability

The Advanced Terrestrial Simulator (ATS) (Coon et al., 2019) is open source under the BSD 3-clause license and is publicly available at https://github.com/amanzi/ats. Simulations were conducted using version 1.2. Forcing data, model input files, Jupyter notebooks used to generate figures, and meshes along with Jupyter notebooks used to generate the meshes are publicly available at https://doi.org/10.5440/1545605.

Supplement

The supplement related to this article is available online at: https://doi.org/xxxxx-supplement.

https://doi.org/10.5194/tc-2023-8
Preprint. Discussion started: 7 February 2023
© Author(s) 2023. CC BY 4.0 License.


Competing interests

The authors declare that they have no conflict of interest.

250 **Acknowledgments**

The Next Generation Ecosystem Experiment (NGEE) Arctic project is supported by the Office of Biological and Environmental Research in the U.S. Department of Energy's Office of Science.

https://doi.org/10.5194/tc-2023-8
Preprint. Discussion started: 7 February 2023
© Author(s) 2023. CC BY 4.0 License.


References

Abolt, C. J., Young, M. H., Atchley, A. L., Harp, D. R., & Coon, E. T. (2020). Feedbacks between surface deformation and permafrost degradation in ice wedge polygons, Arctic Coastal Plain, Alaska. Journal of Geophysical Research: Earth Surface, 125(3), e2019JF005349.

Atchley, A. L., Painter, S. L., Harp, D. R., Coon, E. T., Wilson, C. J., Liljedahl, A. K., & Romanovsky, V. E. (2015). Using field observations to inform thermal hydrology models of permafrost dynamics with ATS (v0. 83). Geoscientific Model Development, 8(9), 2701-2722.

Alduchov, O. A., & Eskridge, R. E. (1996). Improved Magnus form approximation of saturation vapor pressure. Journal of Applied Meteorology and Climatology, 35(4), 601-609.

Brauner, H. (2019). Representation of Spatial Heterogeneity of the Baker Creek Watershed in the Land-Surface Hydrology Model, MESH, M.Sc. thesis, University of Saskatchewan, Canada.

Buck, A. L. (1981). New equations for computing vapor pressure and enhancement factor. Journal of Applied Meteorology and Climatology, 20(12), 1527-1532.

Coon, E., Svyatsky, D., Jan, A., Kikinzon, E., Berndt, M., Atchley, A., ... & Molins, S. (2019). Advanced terrestrial simulator. Computer Software. doi:10.11578/dc.20190911.1

Dessler, A. E., & Sherwood, S. C. (2009). A matter of humidity. Science, 323(5917), 1020-1021.

Gill, A. E. (1982). Atmosphere-ocean dynamics. New York: Academic Press.

Goff, J. A., & Gratch, S. (1946), Low-pressure properties of water from -160 to 212 F, Trans. Am. Soc. Heat. Vent. Eng., 52, 95-121.

Harpold, A. A., & Brooks, P. D. (2018). Humidity determines snowpack ablation under a warming climate. Proceedings of the National Academy of Sciences, 115(6), 1215-1220.

Jan, A., Coon, E. T., & Painter, S. L. (2020). Evaluating integrated surface/subsurface permafrost thermal hydrology models in ATS (v0. 88) against observations from a polygonal tundra site. Geoscientific Model Development, 13(5), 2259-2276.

Leppäranta, M. (2015). Freezing of lakes and the evolution of their ice cover, Springer-Praxis, Heidelberg, Berlin, Germany.

Li, Y., Yao, N., Sahin, S., & Appels, W. M. (2017). Spatiotemporal variability of four precipitation-based drought indices in Xinjiang, China. Theoretical and Applied Climatology, 129(3), 1017-1034.

Liu, T., He, Q., Chen, Y., Liu, J., Liu, Q., Fu, X., ... & Li, R. (2021). Distinct impacts of humidity profiles on physical properties and secondary formation of aerosols in Shanghai. Atmospheric Environment, 267, 118756.

Mackay, S. L., & Marchant, D. R. (2017). Obliquity-paced climate change recorded in Antarctic debris-covered glaciers. Nature communications, 8(1), 1-12.

Murray, F. W. (1967). On the Computation of Saturation Vapor Pressure. Journal of Applied Meteorology and Climatology, 6(1), 203-204.

Nian, D., Linz, M., Mooring, T. A., & Fu, Z. (2022). The changing extreme values of summer relative humidity in the Tarim Basin in northwestern China. Climate Dynamics, 58(11), 3527-3540.

Ruosteenoja, K., Jylhä, K., Räisänen, J., & Mäkelä, A. (2017). Surface air relative humidities spuriously exceeding 100% in CMIP5 model output and their impact on future projections. Journal of Geophysical Research: Atmospheres, 122(18), 9557-9568.

Sexstone, G. A., Clow, D. W., Fassnacht, S. R., Liston, G. E., Hiemstra, C. A., Knowles, J. F., & Penn, C. A. (2018). Snow sublimation in mountain environments and its sensitivity to forest disturbance and climate warming. Water Resources Research, 54(2), 1191-1211.

https://doi.org/10.5194/tc-2023-8
Preprint. Discussion started: 7 February 2023
© Author(s) 2023. CC BY 4.0 License.

Valiantzas, J. D. (2013). Simplified forms for the standardized FAO-56 Penman–Monteith reference evapotranspiration using limited weather data. Journal of Hydrology, 505, 13-23.

Vömel, H. (2016). Saturation vapor pressure formulations. https://sciencepolicy.colorado.edu/~voemel/vp.html Accessed 13/08/2022.

Westermann, S., Langer, M., Boike, J., Heikenfeld, M., Peter, M., Etzelmüller, B., & Krinner, G. (2016). Simulating the thermal regime and thaw processes of ice-rich permafrost ground with the land-surface model CryoGrid 3. Geoscientific Model Development, 9(2), 523-546.

Xie, W., Yi, S., Leng, C., Xia, D., Li, M., Zhong, Z., & Ye, J. (2022). The evaluation of IMERG and ERA5-Land daily precipitation over China with considering the influence of gauge data bias. Scientific Reports, 12(1), 1-21.

Xu, J., Wei, Q., Peng, S., & Yu, Y. (2012). Error of saturation vapor pressure calculated by different formulas and its effect on calculation of reference evapotranspiration in high latitude cold region. Procedia Engineering, 28, 43-48.

https://doi.org/10.5194/tc-2023-8
Preprint. Discussion started: 7 February 2023
© Author(s) 2023. CC BY 4.0 License.

Figures

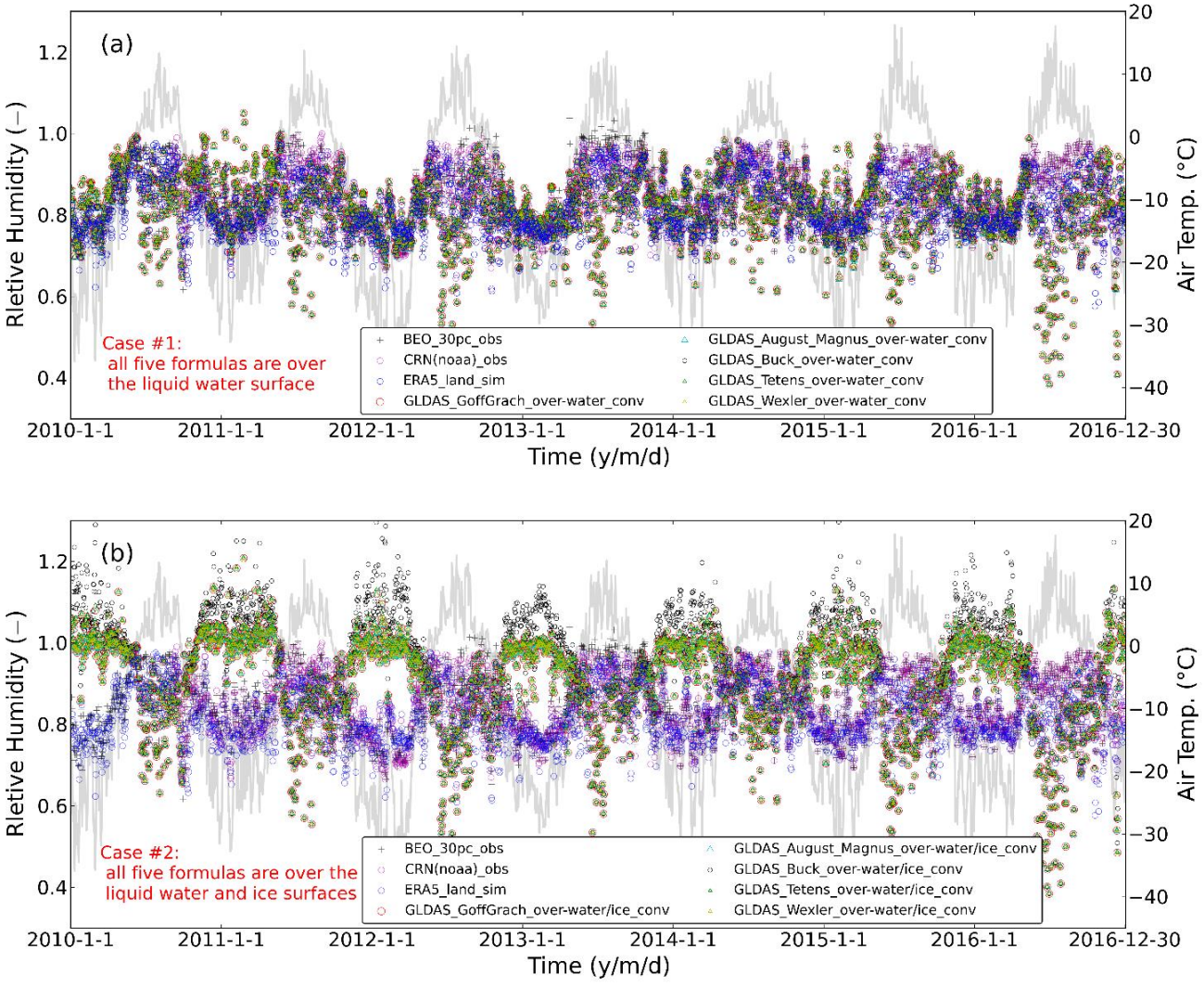

Figure 1: Comparison of the converted RHs based on different formulas over the water (a, Case #1) and over the water/ice (b, Case #2) from the GLDAS dataset vs. the directly downloaded RHs.

https://doi.org/10.5194/tc-2023-8
Preprint. Discussion started: 7 February 2023
© Author(s) 2023. CC BY 4.0 License.

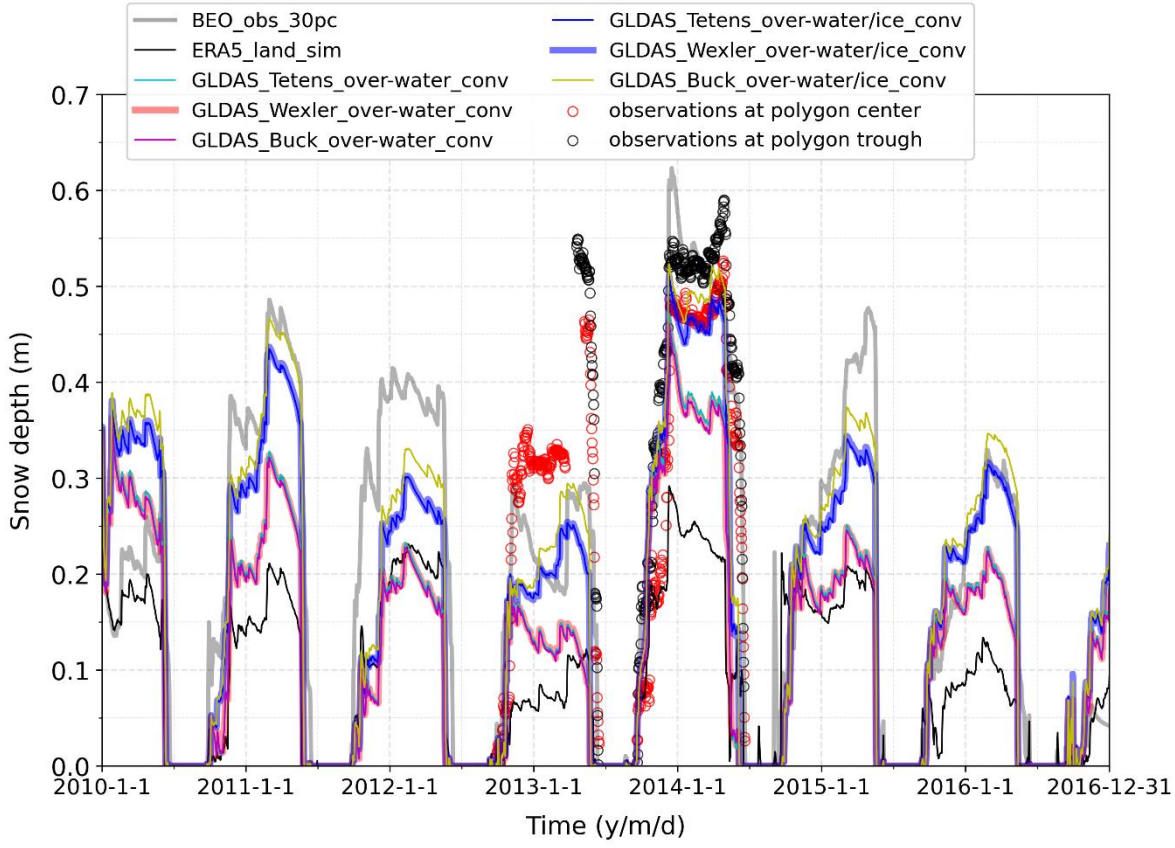

Figure 2: Comparison of the simulated (lines) snow depths and the observations (dots) at Site C (Jan et al., 2020) near Utqiagvik in Alaska (USA). For the BEO observational dataset, the symbol "30pc" means that the snow precipitation includes a 30% adjustment (correction) for undercatch (Atchley et al., 2015; Jan et al., 2020), and the observed snowpacks are collected at the centre and trough of the ice-wedge polygon.

https://doi.org/10.5194/tc-2023-8
Preprint. Discussion started: 7 February 2023
© Author(s) 2023. CC BY 4.0 License.

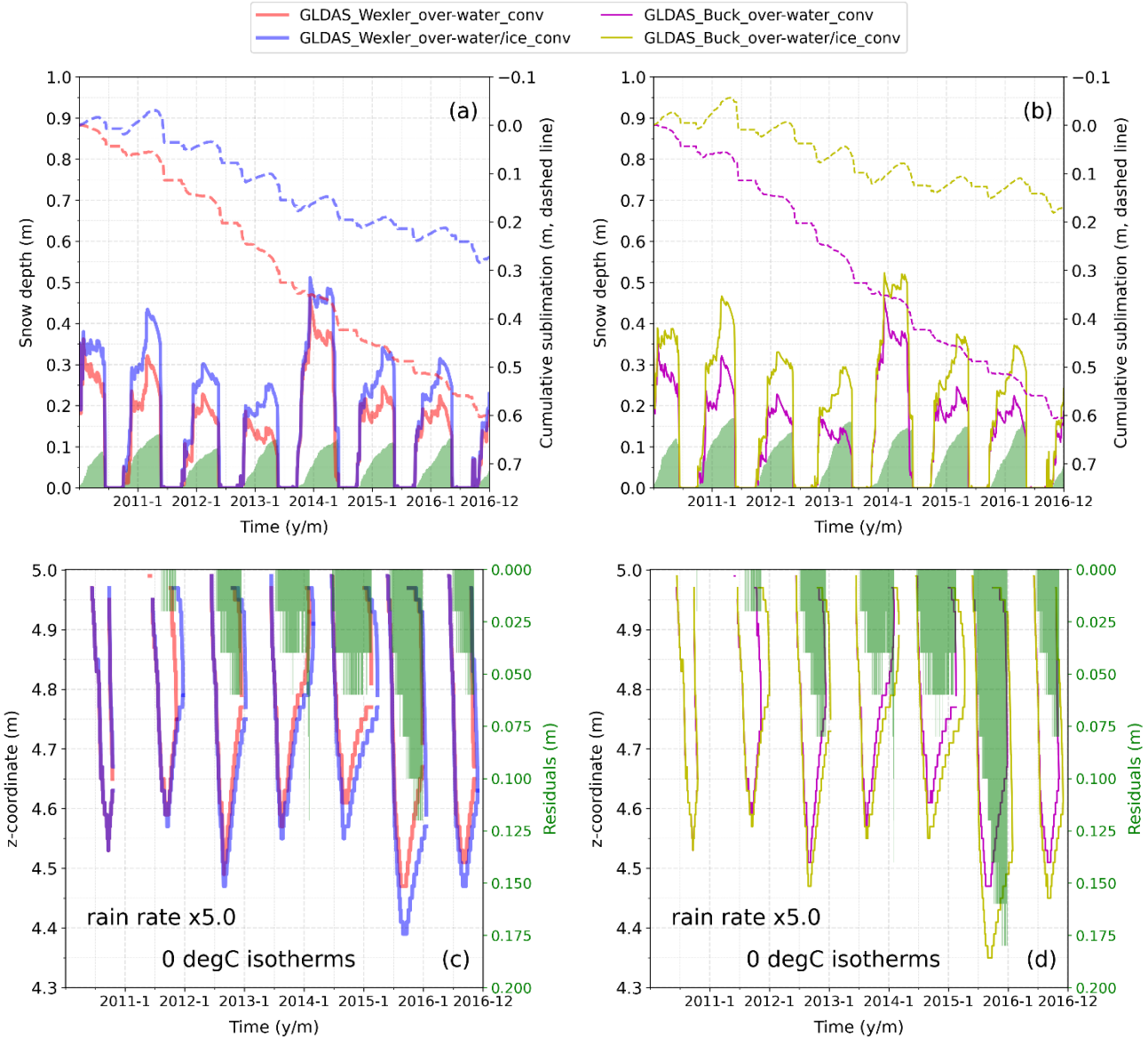

315 **Figure 3:** The top panel is the calculated sublimation using GLDAS dataset by converting the SHs to RHs based on the Wexler formula (a) and the Buck formula (b). The filled areas in green denote the residuals between the simulations with (Case #2) or without (Case #1) over-ice correction of the SVPs. The bottom panel is the propagation of the thawing front using GLDAS dataset by converting the SHs to RHs based on the Wexler formula (c) and the Buck formula (d). The filled areas in shallow green color denote the residuals between them. The rain precipitation rate is increased by five times, and the ponded water depth is constrained to be less than 1.0 m (equal to 1.0 m of seepage
320 water head).